# Enhancement of direct *CP* asymmetry in $Z'$ models

Shireen Niteen Gangal*

*Physical Research Laboratory, Ahmedabad, Gujrat, India;*
*Centre for Excellence in Theoretical and Computational Sciences (CETACS), University of Mumbai, Santacruz East, Mumbai 400098, India*

(Received 21 August 2023; accepted 7 July 2024; published 30 July 2024)

We consider *CP*-violating $Z'$ models to account for the anomalies in $b \to s\ell\ell$ decays. Using the updated constraints from lepton flavor universality violating ratios, $b \to s\mu\mu$ *CP*-conserving and *CP*-violating observables, $B_s - \bar{B}_s$ mixing and neutrino trident we obtain the favored parameter space of two classes of $Z'$ models generating the new physics scenarios with $\mathrm{Re}[C_9^{\mu\mathrm{NP}}] < 0$ and $[C_9^{\mu\mathrm{NP}} = -C_{10}^{\mu\mathrm{NP}}, C_9^{e\mathrm{NP}} = -C_{10}^{e\mathrm{NP}}]$. We study the predictions of direct *CP* asymmetry $A_{CP}$ in $B^+ \to K^+\mu\mu$ decays and *CP* asymmetric angular observables in these models. The favored $1\sigma$ parameter space of $Z'$ models generating scenario $\mathrm{Re}[C_9^{\mu\mathrm{NP}}] < 0$ allows for an enhancement in the integrated $A_{CP}$ in $q^2 = [8, 9]$ GeV$^2$ bin up to $\pm 25\%$, while the $[C_9^{\mu\mathrm{NP}} = -C_{10}^{\mu\mathrm{NP}}, C_9^{e\mathrm{NP}} = -C_{10}^{e\mathrm{NP}}]$ scenario allows only positive values of $A_{CP}$. However, these $A_{CP}$ values flip sign depending on the choice of $J/\psi$ phase, hence distinguishing these two $Z'$ models through a measurement in this bin requires a more reliable determination of the $J/\psi$ phase. The prediction of $A_{CP}$ in the $q^2 = [16, 17]$ GeV$^2$ bin are promising as they allow for an enhancement only in the positive direction for $[C_9^{\mu\mathrm{NP}} = -C_{10}^{\mu\mathrm{NP}}, C_9^{e\mathrm{NP}} = -C_{10}^{e\mathrm{NP}}]$ scenario, irrespective of the choice of strong phase, while both positive and negative values are allowed for the scenario $\mathrm{Re}[C_9^{\mu\mathrm{NP}}]$. We also find that a future more precise measurement of *CP*-asymmetric angular observables $A_8$ and $A_9$ in the low-$q^2$ bins can provide distinguishing signatures of these two $Z'$ models and help constrain new physics *CP*-violating phases.

DOI: 10.1103/PhysRevD.110.015034

## I. INTRODUCTION

There have been discrepancies between the measurements of a few observables in $b \to s\ell\ell$ decays and their Standard Model predictions over the last few years. Among these, the most significant one before the LHCb December 2022 update was the hint of violation of the lepton flavor universality (LFU), which is embedded in the gauge structure of the SM. The LFU has been tested through the measurements of the ratio observables, $R_K = \Gamma(B^+ \to K^+\mu^+\mu^-)/\Gamma(B^+ \to K^+e^+e^-)$ and $R_{K^*} = \Gamma(B^0 \to K^{0*}\mu^+\mu^-)/\Gamma(B^0 \to K^{0*}e^+e^-)$, which were lower than the SM prediction of $\sim 1$ by $3.1\sigma$ and $2.5\sigma$, respectively [1,2] till 2022. However the new measurements of $R_K$ and $R_{K^*}$ by LHCb in December 2022, $R_K = 0.949 \pm 0.047$ and $R_{K^*} = 1.027 \pm 0.076$, are consistent with the SM within $1\sigma$ [3,4]. Though this measurement indicates consistency with electron-muon universality, the branching ratios $\mathrm{BR}(B \to Ke^+e^-)$ are found to be below the SM predictions at the level of $4\sigma$, which may still hint towards presence of new physics. The measurements of LFU ratios defined in the channels $B_d^0 \to K_S^0\mu^+\mu^-$ and $B^+ \to K^{*+}\mu^+\mu^-$ showed deficits, though not so significant, at $1.5\sigma$ [5]. Apart from the LFU ratios, the branching ratio of $B_s \to \phi\mu\mu$ measured by LHCb also exhibits a deficit compared to the SM prediction at the level of $3.5\sigma$ [6,7]. Further, the updated measurement of the angular observable $P_5'$ by LHCb, defined using the fourfold angular distribution of $B_d^0 \to K^{*0}(\to K^+\pi^-)\mu^+\mu^-$ shows a disagreement with the SM prediction at $3.7\sigma$ [8–11].

These anomalies have been addressed in two ways, either using effective field theories (EFT) by including all possible new dimension-six operators, or building specific new physics models. For the EFT analyses, global fits are performed in a model-independent way to all the $b \to s\ell\ell$ data, in order to find the preferred Lorentz structure of the new physics (NP) operators. In the case of one-parameter scenarios, previous global fits have shown a preference to the Wilson coefficient (WC) combinations, $C_9^{\mu\mathrm{NP}} < 0$, or $C_9^{\mu\mathrm{NP}} = -C_{10}^{\mu\mathrm{NP}}$, corresponding to the NP operators $O_9 = (\bar{s}\gamma_\mu P_L b)(\bar{\ell}\gamma^\mu \ell)$ and $O_{10} = (\bar{s}\gamma_\mu P_L b)(\bar{\ell}\gamma^\mu\gamma^5 \ell)$ [12–21]. Although these NP scenarios with real WCs are the

*Contact author: shireen@prl.res.in

preferred ones, in general these NP WCs can also be complex, thereby giving rise to new sources of $CP$ violation. The updated values of $R_{K^{(*)}}$ may imply that the NP in $b \to s\ell\ell$ is of lepton flavor universal nature, i.e., we expect NP effects in both the muonic and electronic WCs of similar magnitudes. However, this need not be the case as was shown in Ref. [22], where complex WCs can give rise to LFU violation and be consistent with the new $R_K$ measurement. Moreover, since $CP$-violating effects in $b \to s$ decays are suppressed in the SM, these are promising channels to look for new sources of $CP$ violation. The new $CP$-violating phases are very weakly constrained as there are only a few measurements of $CP$-violating observables. Global fits with complex NP WCs have been performed in Refs. [14,16,17,23]. The most relevant $CP$-violating observables are mixing-induced $CP$ asymmetry $A_{CP}^{\rm mix}(B_s \to J/\psi\phi)$ and $CP$-asymmetric observables in the $b \to s\ell\ell$ sector. The latter include direct $CP$ violation in $B \to K^{(*)}\mu\mu$, and $CP$-asymmetric angular observables $A_7$, $A_8$, and $A_9$ measured by LHCb [9,24], which still have large uncertainties and are consistent with zero. Taking into account the updated measurement of $R_K$ and $R_{K^*}$, and using constraints from the above $CP$-violating observables in $b \to s\mu\mu$ decays, we perform model-independent global fits to identify the NP scenarios with complex WCs which can provide a good fit to the data.

In the context of models, the two classes proposed to account for these anomalies are $Z'$ models, and models with leptoquarks (LQ). In simplified $Z'$ models, the $Z'$ boson couples to $\bar{s}b$ and muons/electrons at tree level, and can contribute to the scenarios $C_9^{\mu\rm NP} < 0$ and $C_9^{\mu\rm NP} = -C_{10}^{\mu\rm NP}$, while the LQ models can only generate the $C_9^{\mu\rm NP} = -C_{10}^{\mu\rm NP}$ scenario. A few studies in the past obtained constraints on the parameter space of $Z'$ and leptoquark models assuming complex couplings [14,25–27].

In this work, we use direct $CP$ asymmetry in $B^+ \to K^+\mu^+\mu^-$ decays to study the imprints of a class of $CP$-violating $Z'$ models generating the favored scenarios indicated by global fits. The measurement of $A_{CP}$ in $b \to s\ell\ell$ decays is difficult partly because it is very small, and there are asymmetries in production rate and detection efficiencies that affect the measurements. The decay $B \to J/\psi K^*$ which has negligible direct $CP$ asymmetry is used as a control mode to reduce these asymmetries. The LHCb analysis in Ref. [24] is performed in the $0.1 \le q^2 \le 19.0$ GeV$^2$ bin, and the regions near the $\phi(1020)$, $J/\psi$ and $\psi(2S)$ resonances are removed. However, it has been recently shown that the measurement of $A_{CP}$ near the $J/\psi$, $\psi(2S)$ resonances is more interesting as it could lead to a potential large enhancement in the presence of new $CP$-violating phases [28]. Motivated by this, we obtain predictions of $A_{CP}$ in $Z'$ models generating the NP scenarios: $\mathrm{Re}[C_9^{\mu\rm NP}] < 0$ and $[C_9^{\mu\rm NP} = -C_{10}^{\mu\rm NP}, C_9^{e\rm NP} = -C_{10}^{e\rm NP}]$ in order to study the distinguishing features of these two models. For this, we obtain the favored $1\sigma$ parameter space of $Z'$ models with complex couplings, using the updated measurements from $b \to s\ell\ell$ observables, $B_s - \bar{B}_s$ mixing and neutrino trident.

This work is organized as follows. In the next section we perform model-independent global fits to the updated $b \to s\ell\ell$ data to determine the favored NP scenarios. In Sec. III, we consider the effective Hamiltonian for $b \to s\ell\ell$ decays and define the NP WCs $C_9^{\rm NP}$ and $C_{10}^{\rm NP}$ in terms of the $Z'$ couplings, through matching. In Sec. IV, we list the measurements that constrain the complex $Z'$ couplings. In Sec. V, we discuss how we parametrize the region near charmonium resonance, and present the predictions of integrated $A_{CP}$ in the allowed parameter space of the $Z'$ model. We conclude in Sec. VI.

## II. MODEL-INDEPENDENT GLOBAL FITS

Recently the experimental picture of $b \to s\ell\ell$ anomalies changed considerably, with the LFU ratios meaasured by LHCb and the $\mathrm{BR}(B_s \to \mu^+\mu^-)$ measured by CMS converging with the SM predictions. In this section, we briefly reaccess the status of NP effects in $b \to s\ell\ell$ decays, considering '1D' NP scenarios with complex WCs. We include the following $CP$-conserving and $CP$-violating observables: LFU ratios: $R_K$ and $R_{K^*}$ in $q^2 = (1.1\text{–}6.0)$ GeV$^2$, and $q^2 = (0.1\text{–}1.1)$ GeV$^2$ bins [3,4].

(i) Angular Observables: Longitudinal polarization fraction $F_L$, forward-backward asymmetries $A_{FB}$, and optimized observables $S_3$, $S_4$, $S_5$, $S_7$, $S_8$, $S_9$, in various $q^2$ bins by LHCb [9,10], $F_L$, $P_1$, $P_4'$, $P_5'$, $P_6'$, $P_8'$ by ATLAS [29], $P_1$, $P_5'$, $F_L$ and $A_{FB}$ by CMS [30].

(ii) Branching Ratios: $B_s \to X_s\mu\mu$ [31], $B_s \to \mu\mu$ [32], $B_s \to \phi\mu\mu$ [7], differential branching ratios of $B^0 \to K^{(*)0}\mu\mu$, $B^+ \to K^{(*)+}\mu\mu$ [33,34] in different $q^2$ bins.

(iii) $CP$-violating angular observables: Angular asymmetries $A_3, A_4, A_5, A_{6s}, A_7, A_8, A_9$ in $B^0 \to K^{*0}\mu\mu$ in different $q^2$ bins [9,24].

(iv) $b \to se^+e^-$ observables: $P_4'$, $P_5'$, $F_L$ in $B^0 \to K^{*0}ee$, $\mathrm{BR}(B^0 \to K^{*0}ee)$, $\mathrm{BR}(B^+ \to K^+ee)$, and $\mathrm{BR}(B \to X_see)$ [4,31,35,36].

We follow the fit methodology adopted in Ref. [15]. Since the $Z'$ couplings are complex we include in the fit additional constraints from $CP$-asymmetric angular observables measured by LHCb [9]. The $\chi^2$ function for the $b \to s\mu^+\mu^-$ observables is given by

$$\chi^2_{b\to s\mu\mu}(C_i) = [\mathcal{O}_{\rm th}(C_i) - \mathcal{O}_{\rm exp}]^T \mathcal{C}^{-1} [\mathcal{O}_{\rm th}(C_i) - \mathcal{O}_{\rm exp}], \quad (1)$$

where $C_i = C_{9,10}^{\rm NP}$. The theoretical predictions of $b \to s\mu^+\mu^-$ observables calculated using `flavio` [37] are denoted by $\mathcal{O}_{\rm th}(C_i)$ and the corresponding experimental measurements by $\mathcal{O}_{\rm exp}$. The total covariance matrix $\mathcal{C}$ is obtained by adding

TABLE I. The best fit values of new WCs in various 1D and 2D scenarios. Here $\Delta\chi^2 = \chi^2_{\rm SM} - \chi^2_{\rm bf}$ where $\chi^2_{\rm bf}$ is the $\chi^2$ at the best-fit point and $\chi^2_{\rm SM}$ corresponds to the SM.

| Scenario | Best-fit value(s) | Pull $= \sqrt{\Delta\chi^2_{2023}}$ | p-value |
|---|---|---|---|
| I: $\mathrm{Re}[C_9^{\mu,\mathrm{NP}}] < 0$ | $(-0.64 \pm 0.17) + (1.4 \pm 0.3)I$ | 4.0 | 0.28 |
| II: $C_9^{\mu,\mathrm{NP}} = -C_{10}^{\mu,\mathrm{NP}}$ | $(-0.21 \pm 0.12) + (-0.75 \pm 0.55)I$ | 2.8 | 0.16 |
| III: $C_9^{\mu,\mathrm{NP}} = -C_{10}^{\mu,\mathrm{NP}}$, $C_9^{e,\mathrm{NP}} = -C_{10}^{e,\mathrm{NP}}$ | $(-0.51 - 0.67I, -0.38)$ | 4.1 | 0.27 |
| IV: $C_9^{\mu,\mathrm{NP}} = -C_{10}^{\mu,\mathrm{NP}}$, $C_9^{e,\mathrm{NP}} = C_{10}^{e,\mathrm{NP}}$ | $(-0.22 - 0.71I, 0.32)$ | 3.0 | 0.16 |
| V: $C_9^{\mu,\mathrm{NP}} = C_9^{e,\mathrm{NP}} < 0$ | $(-1.02 \pm 0.18) + (0.15 \pm 0.73)I$ | 5.0 | 0.46 |

the individual theoretical and experimental covariance matrices.

The fit results with this updated data are shown in Table I for the scenarios $\mathrm{Re}[C_9^{\mu\mathrm{NP}}] < 0$ and $C_9^{\mu\mathrm{NP}} = -C_{10}^{\mu\mathrm{NP}}$, which were favored prior to the $R_K$ update. We also consider additional scenarios where NP is present in both muon and electron sectors; $[C_9^{\mu\mathrm{NP}} = -C_{10}^{\mu\mathrm{NP}}, C_9^{e\mathrm{NP}} = \pm C_{10}^{e\mathrm{NP}}]$ and LFU case $C_9^{\mu\mathrm{NP}} = C_9^{e\mathrm{NP}}$. For simplicity, we assumed the NP couplings in the electron sector to be real in Scenarios III and IV. The $\chi^2$ of SM is $\chi^2_{\rm SM} = 194.4$, for 171 degrees of freedom corresponding to a p-value of 0.10.

The overall significance of NP has reduced compared to previous fit results due to the value of $R_K$ and $R_{K^*}$ converging towards SM predictions. We find that the then favored scenario $\mathrm{Re}[C_9^{\mu\mathrm{NP}}] < 0$ still improves the fit compared to the SM, with $\chi^2_{\rm NP} = 178.5$ and a p-value of 0.27. The significance of the scenario $C_9^{\mu\mathrm{NP}} = -C_{10}^{\mu\mathrm{NP}}$ has reduced compared to $\mathrm{Re}[C_9^{\mu\mathrm{NP}}] < 0$ due to the little space left for NP in $C_{10}^{\mu\mathrm{NP}}$ by the new measurement of $B_s \to \mu^+\mu^-$. The scenario $[C_9^{\mu\mathrm{NP}} = -C_{10}^{\mu\mathrm{NP}}, C_9^{e\mathrm{NP}} = -C_{10}^{e\mathrm{NP}}]$ provides an equally good fit to the data as $\mathrm{Re}[C_9^{\mu\mathrm{NP}}] < 0$. Scenario $C_9^{\mu\mathrm{NP}} = C_9^{e\mathrm{NP}}$ with LFU couplings to both electron and muon channels, provides a very good fit to the data, as the recent RK update indicates electron-muon universality.

The $R_K$ and $R_{K^*}$ measurements drive the fit pulling the best-fit value of $\mathrm{Re}[C_9^{\mu\mathrm{NP}}]$ towards 0, from the older values which were close to $-1$. The measurement of $B \to K^*\mu\mu$ observables prefer larger negative $\mathrm{Re}[C_9^{\mu\mathrm{NP}}]$ values. The discrepancy of the branching ratio $B_s \to \phi\mu^+\mu^-$ measurement compared with the SM prediction causes the NP Scenarios I and III, to have larger pulls. For Scenarios II and III, the negative values of $\mathrm{Im}[C_9^{\mu\mathrm{NP}}]$ are due to the measurements of $A_{7,8,9}$ observables. The observables in the electron sector, constrain the NP electron couplings to smaller negative values.

## III. THE $Z'$ MODEL AND $b \to s\ell\ell$ TRANSITIONS

The effective Hamiltonian for $b \to s\ell\ell$ transitions is given by

$$\begin{aligned}\mathcal{H}_{\rm eff}^{b\to\ell\ell} = -\frac{4G_F}{\sqrt{2}} V_{ts}^* V_{tb} \Bigg[ & \sum_{i=1}^{6} C_i \mathcal{O}_i \\ & + C_7^{\rm SM} \frac{e}{16\pi^2} [\bar{q}\sigma_{\mu\nu}(m_s P_L + m_b P_R) b] F^{\mu\nu} + C_8 \mathcal{O}_8 \\ & + C_9 \frac{\alpha_{\rm em}}{4\pi} (\bar{s}\gamma^\mu P_L b)(\bar{\ell}\gamma_\mu \ell) \\ & + C_{10} \frac{\alpha_{\rm em}}{4\pi} (\bar{s}\gamma^\mu P_L b)(\bar{\ell}\gamma_\mu\gamma_5 \ell) \Bigg] + \mathrm{H.c.}, \end{aligned} \tag{2}$$

where $G_F$ is the Fermi constant and $V_{ij}$ are the Cabibbo-Kobayashi-Maskawa (CKM) matrix elements. The contribution from the operators $O_{i=1\ldots6}$ are included through the modification, $C_{7,8,9}^{\rm SM} \to C_{7,8,9}^{\rm eff,SM}$. The presence of new physics modifies the WCs corresponding to semileptonic operators $O_9$ and $O_{10}$ as follows: $C_9 = C_9^{\rm eff,SM} + C_9^{\ell,\mathrm{NP}}$ and $C_{10} = C_{10}^{\rm eff,SM} + C_{10}^{\ell,\mathrm{NP}}$, where $\ell = \mu, e$.

The NP contribution to $B_s - \bar{B}_s$ mixing can be parametrized by the effective Hamiltonian,

$$\mathcal{H}_{\rm eff}^{\Delta B=2} = -\frac{4G_F}{\sqrt{2}} V_{tb} V_{ts}^* (C_1^{bs} (\bar{s}\gamma_\mu b)^2) + \mathrm{H.c.}, \tag{3}$$

where $C_1^{bs}$ is modified as, $C_1^{bs} = C_1^{bs,\rm SM} + C_1^{bs,\mathrm{NP}}$.

The couplings of a generic $Z'$ model relevant for $b \to s\ell\ell$ decays are given by

$$\begin{aligned}\mathcal{L}_{Z'} \supset & Z_\alpha J_{Z'}^\alpha \\ & = (g_L^\mu \bar{L}_2 \gamma^\alpha P_L L_2 + g_R^\mu \bar{e}_2 \gamma^\alpha P_R e_2 + g_L^{bs} \bar{s}\gamma^\alpha P_L b) Z'_\alpha \\ & \quad + (g_L^e \bar{L}_1 \gamma^\alpha P_L L_1 + g_R^e \bar{e}_1 \gamma^\alpha P_R e_1) Z'_\alpha, \end{aligned} \tag{4}$$

where $L_2(e_2)$ and $L_1(e_1)$ are the second and first generation lepton doublets (singlets), respectively, $g_L^\mu(g_R^\mu)$ are left-handed (right-handed) couplings of $Z'$ to muons and electrons, respectively, while $g_L^{bs}$ are couplings to quarks. We only consider left-handed couplings in the quark sector. Since the $Z'$ is much heavier, it can be integrated out to get an effective Hamiltonian with relevant four fermion interactions given by

$$\begin{aligned}\mathcal{H}_{\text{eff}}^{Z'} &= \frac{1}{2M_{Z'}^2} J_\alpha J^\alpha \\ &= \frac{g_L^{bs}}{M_{Z'}^2}(\bar{s}\gamma^\alpha P_L b)[\bar{\mu}\gamma_\alpha(g_L^\mu P_L + g_R^\mu P_R)\mu] \\ &+ \frac{g_L^{bs}}{M_{Z'}^2}(\bar{s}\gamma^\alpha P_L b)[\bar{e}\gamma_\alpha(g_L^e P_L + g_R^e P_R)e] \\ &+ \frac{(g_L^{bs})^2}{2M_{Z'}^2}(\bar{s}\gamma^\alpha P_L b)(\bar{s}\gamma_\alpha P_L b) \\ &+ \frac{g_L^\mu}{M_{Z'}^2}(\bar{\nu}_\mu\gamma_\alpha P_L\nu_\mu)[\bar{\mu}\gamma^\alpha(g_L^\mu P_L + g_R^\mu P_R)\mu]. \quad (5)\end{aligned}$$

Here, the first two terms contribute to $b \to s\ell\ell$ transitions, the third term to $B_s - \bar{B}_s$ mixing and the last term to neutrino trident production $\nu_\mu N \to \nu_\mu N\mu^+\mu^-$.

The results of updated global fits in Table I, indicate that the most preferred scenarios are Scenario I: $\text{Re}[C_9^{\mu,\text{NP}}] < 0$, Scenario III: $[C_9^{\mu\text{NP}} = -C_{10}^{\mu\text{NP}}, [C_9^{e\text{NP}} = -C_{10}^{e\text{NP}}]$, and Scenario IV: $C_9^{\mu\text{NP}} = C_9^{e\text{NP}} < 0$. We consider the two favored NP Scenarios I and III that can be generated in $Z'$ models. A $Z'$ that couples to muons through $L_\mu - L_\tau$ portal can generate Scenario I [38]. For Scenario III, we consider a generic $Z'$ model that has left-handed couplings to both electrons and muons [39].

In a $Z'$ model generating Scenario I, the SM is extended by a new Abelian $U(1)'$ gauge group and the $Z'$ is the associated massive vector boson. While the leptonic part of the current is same as Eq. (4), the hadronic part is given by

$$J_{Z'}^{\alpha,\text{had}} = L_{ij}^d \bar{d}_i\gamma^\alpha P_L d_j + L_{ij}^u \bar{u}_i\gamma^\alpha P_L u_j, \quad (6)$$

where $L_{ij} = \lambda_{ij} v_\phi^2/\Lambda^2$, where $v_\phi$ is the vacuum expectation values of the scalar field $\Phi$ that Higgses the $U(1)'$ and gives mass to the $Z'$ boson. To explain the anomalies in $b \to s\ell\ell$, the $Z'$ needs to couple to quarks through heavy vectorlike quarks. The Yukawa couplings of heavy vectorlike quarks with the SM quarks and the field $\Phi$ introduce the couplings of $Z'$ with the SM quarks. Integrating out the heavy vectorlike quarks, the WCs relevant for $b \to s\ell\ell$ decays and $B_s$ mixing can be obtained as follows [38]:

$$\begin{aligned}C_9^{\mu\text{NP}} &= \frac{-\pi}{\sqrt{2}G_F\alpha V_{tb}V_{ts}^*}\frac{(Y_{Qb}Y_{Qs}^*)g_L^\mu}{2m_Q^2}, \\ C_{10}^{\mu\text{NP}} &= \frac{\pi}{\sqrt{2}G_F\alpha V_{tb}V_{ts}^*}\frac{(Y_{Qb}Y_{Qs}^*)g_L^\mu}{2m_Q^2}, \\ C_1^{bs} &= \frac{(Y_{Qb}Y_{Qs}^*)^2}{m_Q^2(V_{tb}V_{ts}^*)^2}\left[\frac{v_\phi^2}{m_Q^2}\frac{1}{16\sqrt{2}G_F} + \frac{1}{16^2\pi^2\sqrt{2}G_F}\right], \quad (7)\end{aligned}$$

where $Y_{Qb(s)}$ is the Yukawa coupling due to the mixing of the vectorlike quarks with the SM quark, and $m_Q$ is the mass of the vectorlike quarks.

In a generic $Z'$ model with couplings to both muons and electrons, the NP WCs can be obtained by matching Eq. (5) on to the $b \to s\ell\ell$ effective Hamiltonian Eq. (2),

$$C_9^{\mu(e),\text{NP}} = -\frac{\pi}{\sqrt{2}G_F\alpha V_{tb}V_{ts}^*}\frac{g_L^{bs}\left(g_L^{\mu(e)} + g_R^{\mu(e)}\right)}{M_{Z'}^2}, \quad (8)$$

$$C_{10}^{\mu(e),\text{NP}} = \frac{\pi}{\sqrt{2}G_F\alpha V_{tb}V_{ts}^*}\frac{g_L^{bs}\left(g_L^{\mu(e)} - g_R^{\mu(e)}\right)}{M_{Z'}^2}, \quad (9)$$

$$C_1^{bs} = \frac{1}{4\sqrt{2}G_F M_{Z'}^2}\left(\frac{g_L^{bs}}{V_{tb}V_{ts}^*}\right)^2. \quad (10)$$

For Scenario III, we require $g_R^e,\ g_R^\mu = 0$.

## IV. CONSTRAINTS

The observables in $b \to s\mu^+\mu^-$ sector constrain the product of the couplings $g_L^{bs}g_{L,R}^\mu$. The $Z'$ quark coupling $g_L^{bs}$ receives strong constraints from the measurement of $B_s - \bar{B}_s$ mixing through the expression [25],

$$\frac{\Delta M_s^{\text{SM+NP}}}{\Delta M_s^{\text{SM}}} = \left|1 + \frac{\eta^{6/23}}{R_{\text{loop}}^{\text{SM}}}C_1^{bs}\right|, \quad (11)$$

where $\eta = \alpha_s(\mu_{NP})/\alpha_s(m_b)$ and

$$R_{\text{loop}}^{\text{SM}} = \frac{\sqrt{2}G_F M_W^2\eta_B S_0(x_t)}{16\pi^2} = 1.31 \times 10^{-3}. \quad (12)$$

The measurement of mixing-induced $CP$ asymmetry in $B_s \to J/\psi\phi$ can be used to constrain $\text{Im}[g_L^{bs}]$, which in the presence of NP is given by

$$A_{CP}^{\text{mix}} = \sin(\phi_\delta - 2\beta_s), \quad (13)$$

where

$$\phi_\delta = \arg\left(1 + \frac{C_1^{bs}}{R_{\text{loop}}^{\text{SM}}}\right). \quad (14)$$

The lepton couplings $g_{L,R}^\mu$ can also be constrained using neutrino trident production $\nu_\mu N \to \nu_\mu N\mu^+\mu^-$, since by $SU(2)_L$ invariance the $Z'$ couples with neutrinos via the same coupling as muons. The cross section for neutrino trident can be parametrized as [14]

$$\begin{aligned}R_\nu = \frac{\sigma}{\sigma_{\text{SM}}} = \frac{1}{1 + (1 + 4s_W^2)^2}\Bigg[&\left(1 + \frac{v^2 g_L^\mu(g_L^\mu - g_R^\mu)}{M_{Z'}^2}\right)^2 \\ &+ \left(1 + 4s_W^2 + \frac{v^2 g_L^\mu(g_L^\mu + g_R^\mu)}{M_{Z'}^2}\right)^2\Bigg], \quad (15)\end{aligned}$$

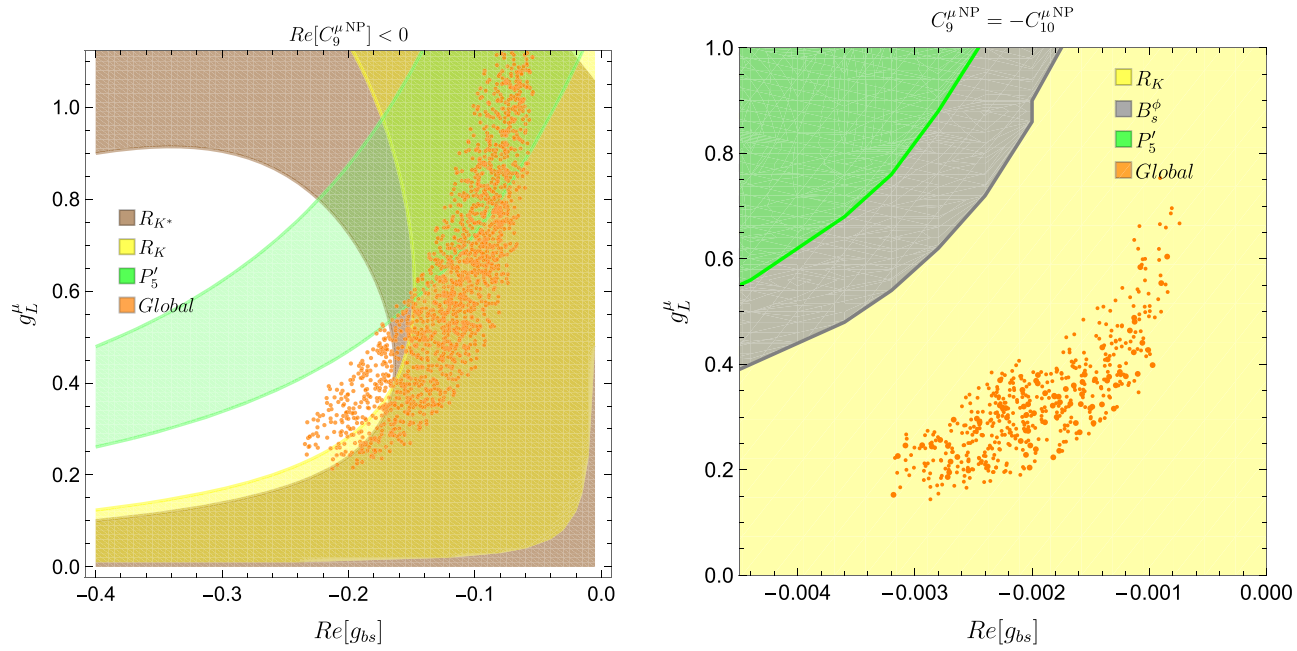


FIG. 1. The $1\sigma$ allowed region (orange) in the parameter space of $\mathrm{Re}[g_L^{bs}]$ and $g_L^\mu$ couplings for $Z'$ models generating scenarios with $\mathrm{Re}[C_9^{\mu\mathrm{NP}}] < 0$ (left) and $[C_9^{\mu\mathrm{NP}} = -C_{10}^{\mu\mathrm{NP}}, C_9^{e\mathrm{NP}} = -C_{10}^{e\mathrm{NP}}]$ (right). The $1\sigma$ range from experimental measurements of $R_K$, $R_{K^*}$, $P_5'$, and $\mathrm{Br}(B_s \to \phi\mu\mu)$ are also shown.

where $v = 246$ GeV, $s_W = \sin\theta_W$, and we use $R_\nu^{\mathrm{exp}} = 0.82 \pm 0.28$ [40,41].

We also include LEP-II constraints using the $e^+e^- \to \mu^+\mu^-$ channel [42], to constrain $Z'$ electron-muon couplings in Scenario III. Since the $Z'$ in Scenario I does not couple to electrons, these LEP constraints do not apply.

Combining the constraints from the above measurements, we find the best-fit values for the $Z'$ couplings, assuming $M_{Z'} = 1$ TeV, to be

$$(g_L^{bs}, g_L^\mu) = \{-0.16 - 0.046I, 0.38)\},$$
$$(g_L^{bs}, g_L^\mu, g_L^e) = \{(-1.5 - 1.8I) \times 10^{-3}, 0.5, 0.45)\}, \quad (16)$$

for Scenarios I and III, respectively.

Figure 1 depicts the $1\sigma$ favored region in the parameter space of quark coupling $\mathrm{Re}[g_{bs}]$ and muon coupling $g_L^\mu$ for $\mathrm{Re}[C_9^{\mu\mathrm{NP}}] < 0$ (left) and $C_9^{\mu\mathrm{NP}} = -C_{10}^{\mu\mathrm{NP}}, C_9^{e\mathrm{NP}} = -C_{10}^{e\mathrm{NP}}$ scenarios (right). The NP $Z'$ couplings improve the fit, with $\Delta\chi^2 = \chi^2_{\mathrm{SM}} - \chi^2_{\mathrm{NP}} \sim 18$ and $\Delta\chi^2 = 20$ for Scenarios I and III, respectively. The global $1\sigma$ favored region shown in orange is consistent with the $1\sigma$ bounds from measurements of $R_K$, $R_{K^*}$, and $P_5'$ in Scenario I but it cannot account for the branching ratio of $B_s \to \phi\mu\mu$. The $1\sigma$ bounds on the measurement of $\mathrm{Br}(B_s \to \phi\mu\mu)$ require larger negative $C_9^{\mu\mathrm{NP}} \gtrapprox -1$ [15], while the current data driven by $R_{K^{(*)}}$ measurements prefer much smaller $C_9^{\mu\mathrm{NP}}$ values (see Table I).

The $1\sigma$ favored region in Scenario III cannot account for the measurements of both $P_5'$ and the branching ratio of $B_s \to \phi\mu\mu$ within $1\sigma$. These measurements require larger values of $g_L^\mu$ and $\mathrm{Re}[g_{bs}]$. However, the measurement of $\mathrm{Br}(B_s \to \mu^+\mu^-)$ being consistent with the SM predictions pull the global fit towards smaller values of $\mathrm{Re}[g_{bs}]$, creating a tension between the global fit $1\sigma$ region and the experimental $1\sigma$ regions of $P_5'$ and $\mathrm{Br}(B_s \to \phi\mu\mu)$. Further, the LEP-II measurements constrain $g_L^\mu$ and $g_L^e$ to smaller values. Note that due to the additional electron couplings in Scenario III, the entire parameter space of $g_L^\mu$ is allowed by the measurement of $R_K$ and $R_{K^*}$.

In Fig. 2 we show the $1\sigma$ favored region in the space of complex $Z'$ quark couplings for Scenarios I (left) and III (right). Marginalizing over $g_L^\mu$, we find that the favored $1\sigma$ region in the plane of $\mathrm{Re}[g_{bs}] - \mathrm{Im}[g_{bs}]$ is consistent with the $1\sigma$ bounds from $P_5'$, $R_K$, $A_{CP}^{\mathrm{mix}}$, and $\Delta M_s$, but not $\mathrm{Br}(B_s \to \phi\mu\mu)$ for Scenario I. The favored region in Scenario III is also consistent with $P_5'$, $R_K$, $A_{CP}^{\mathrm{mix}}$, and $\Delta M_s$ measurements, and partly with the measurement of $\mathrm{Br}(B_s \to \phi\mu\mu)$, though this region requires larger values of $\mathrm{Re}[g_{bs}]$. Hence, there are some tensions between the global $1\sigma$ regions shown in orange, and some measurements like $\mathrm{Br}(B_s \to \phi\mu\mu)$, as the global fit for complex $Z'$ couplings is mainly driven by $R_{K^{(*)}}$, $\Delta M_s$ and $A_{CP}^{\mathrm{mix}}$ measurements in both Scenarios I and III.

We note that the strongest bound on the imaginary part of these $Z'$ quark couplings come from the measurements of $\Delta A_{CP}^{\mathrm{mix}}$, still allowing imaginary couplings as large as the real

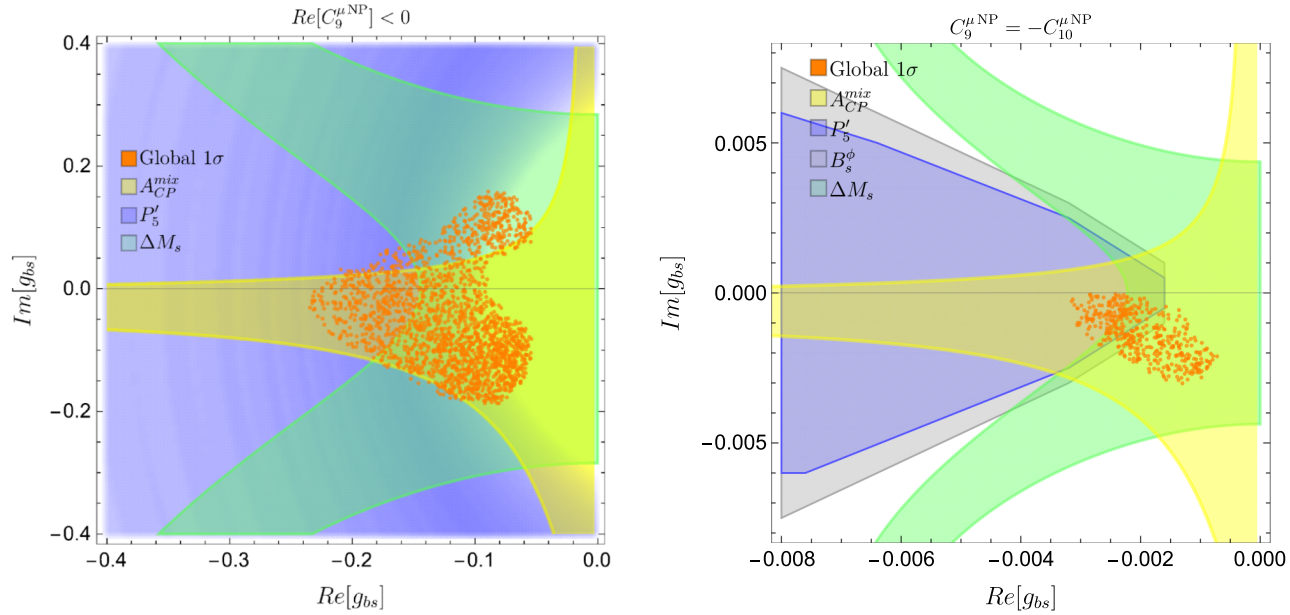


FIG. 2. The $1\sigma$ allowed region (orange) in the parameter space of complex $g_L^{bs}$ coupling for $Z'$ models generating scenarios with $\mathrm{Re}[C_9^{\mu\mathrm{NP}}] < 0$ (left) and $[C_9^{\mu\mathrm{NP}} = -C_{10}^{\mu\mathrm{NP}}, C_9^{e\mathrm{NP}} = -C_{10}^{e\mathrm{NP}}]$ (right). The $1\sigma$ constraints from $B_s$ mixing observable $\Delta M_s$, mixing induced $CP$ asymmetry $A_{CP}^{\mathrm{mix}}$, $P_5'$, and $\mathrm{Br}(B_s \to \phi\mu\mu)$ are also shown.

ones. We use the ratio $\Delta M_s^{\mathrm{SM}}/\Delta M_s^{\mathrm{exp}} = 1.04 \pm 0.07$ [25], which corresponds to the current experimental value of $\Delta M_s^{\mathrm{exp}} = 17.757 \pm 0.021$, and the SM prediction given by the weighted average of sum rule and FLAG 2019 prediction, $\Delta M_s^{\mathrm{SM}} = (18.4 \pm 1.2)\ \mathrm{ps}^{-1}$. The preference to $\mathrm{Im}[C_9^{\mathrm{NP}}]$ is more pronounced in the case of FLAG 2019 SM prediction, $\Delta M_s^{\mathrm{SM}} = (20.1 \pm 1.6)\ \mathrm{ps}^{-1}$ which has a much higher central value than the weighted average. The bounds from $CP$-asymmetric angular observables $A_7$, $A_8$, $A_9$, show some preference towards $\mathrm{Im}[C_9^{\mathrm{NP}}] < 0$, and this is more prominent in the case of Scenario III which shifts the best-fit towards larger negative $\mathrm{Im}[g_{bs}]$ values, as can be seen in Fig. 2.

## V. $A_{CP}$ PREDICTIONS

We now study the implications of complex $Z'$ couplings on the predictions of direct $CP$ asymmetry in $B^+ \to K^+\mu^+\mu^-$ decays. Since the SM prediction of $A_{CP}$ is very small $O(10^{-3})$, a nonzero measurement of $A_{CP}$ could indicate presence of new physics. The direct $CP$ asymmetry is defined as

$$A_{CP}(q^2) = \frac{d\bar{\Gamma}(B^- \to K^-\mu\mu)/dq^2 - d\Gamma(B^+ \to K^+\mu\mu)/dq^2}{d\bar{\Gamma}(B^- \to K^-\mu\mu)/dq^2 + d\Gamma(B^+ \to K^+\mu\mu)/dq^2}, \tag{17}$$

where the differential decay rate for $B^+ \to K^+\mu\mu$ and the corresponding form factors are taken from Ref. [43].

A nonzero $A_{CP}$ requires an interference between two amplitudes with different strong and weak phases. This is possible due to an interference between the phase of the $Z'$ couplings and the strong phases in the $c\bar{c}$ resonance region. The effect of the presence of $c\bar{c}$ resonances enter via the process $B \to V_{c\bar{c}} \to \ell\ell$, where $V_{c\bar{c}}$ can be any of $J/\psi, \psi(2S), \psi(3770), \psi(4040), \psi(4160)$, or $\psi(4415)$. These long-distance effects can be modeled theoretically via a sum over Breit-Wigner (BW) poles as follows [44]:

$$C_9 \to C_9 - \frac{9\pi}{\alpha^2}\bar{C}\sum_V |\eta_V| e^{i\delta_V} \frac{\hat{m}_V \mathcal{B}(V \to \mu^+\mu^-)\hat{\Gamma}_{\mathrm{tot}}^V}{\hat{q}^2 - \hat{m}_V^2 + i\hat{m}_V\hat{\Gamma}_{\mathrm{tot}}^V}, \tag{18}$$

where $\bar{C} = \bar{C}_1 + \bar{C}_2/3 + \bar{C}_3 + \bar{C}_4/3 + \bar{C}_5 + \bar{C}_6/3$ and $|\eta_V|$ is the magnitude of the resonances. The masses, branching ratios and decay widths of the resonances are taken from Ref. [45]. We use $C_9^{\mathrm{SM}} = C_9^{\mathrm{eff}} = C_9 + Y(q^2)$ where $Y(q^2)$ is taken from Refs. [46,47]. The values of the strong phases $\delta_j$ and their magnitude $\eta_j$ are taken from LHCb analysis [48], wherein these phases were determined through a fit to the full dimuon mass spectrum, using a model for the resonances in the form of a Breit-Wigner function. The fit leads to four possible combinations such that the sign of the phase of $J/\psi$ is negative (Branch A) or positive (Branch B), and the $\psi(2S)$ phase can have either sign. The best fit values of these phases are

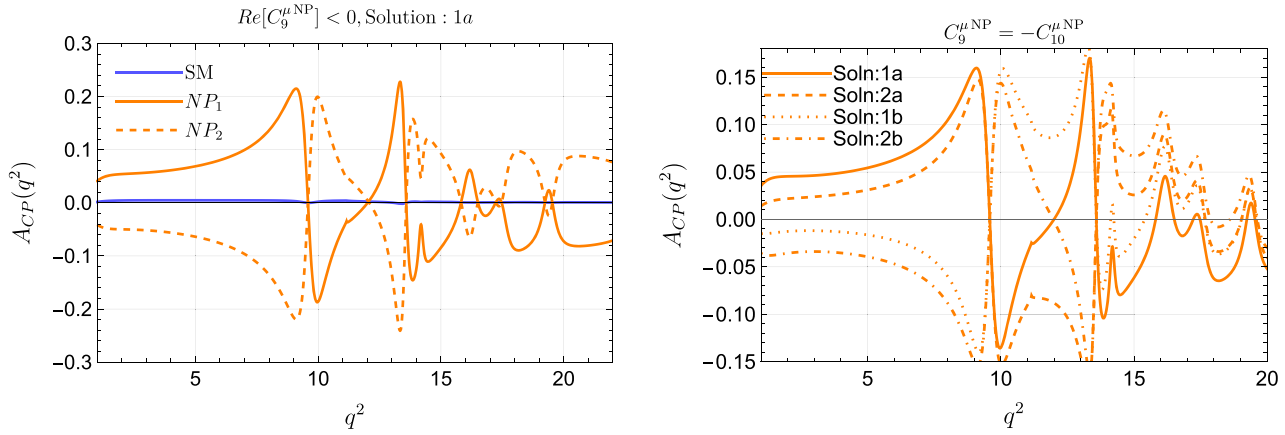


FIG. 3. Predictions of $A_{CP}(q^2)$ in the full $q^2$ region for the two maximal benchmark points NP1: $C_9^{\mu\mathrm{NP}} = -0.56 - 1.1i$ and NP2: $C_9^{\mu\mathrm{NP}} = -0.67 + 1.1i$ in Scenario I (left panel). Predictions of $A_{CP}$ in Scenario III for $C_9^{\mu\mathrm{NP}} = -C_{10}^{\mu\mathrm{NP}} = -0.3 - 0.8i$ (right panel), for all four phase choices.

$$\begin{aligned}&\text{Branch A:}\\&\text{Solution 1a: } \delta_{J/\psi} = -1.66, \quad \delta_{\psi(2S)} = -1.93,\\&\text{Solution 2a: } \delta_{J/\psi} = -1.50, \quad \delta_{\psi(2S)} = 2.08. \end{aligned} \tag{19}$$

$$\begin{aligned}&\text{Branch B:}\\&\text{Solution 1b: } \delta_{J/\psi} = 1.47, \quad \delta_{\psi(2S)} = -2.21,\\&\text{Solution 2b: } \delta_{J/\psi} = 1.63, \quad \delta_{\psi(2S)} = 1.80. \end{aligned} \tag{20}$$

In Fig. 3, we show the predictions of $A_{CP}(q^2)$ in the full $q^2$ region for Scenario I considering Solution 1a as the phase choice (left panel), and Scenario III with all four phase choices (right panel).

To get an estimate of the maximum deviation in $A_{CP}(q^2)$ we consider the following two benchmark points in Scenario I corresponding to the maximum allowed values of $\mathrm{Im}[g_{bs}]$ within $1\sigma$:

(i) NP1: $(g_L^{bs}, g_L^{\mu}) = \{(-0.1 - 0.19i), 0.68\}$
(ii) NP2: $(g_L^{bs}, g_L^{\mu}) = \{(-0.09 + 0.15i), 0.89\}$

These benchmark points correspond to $C_9^{\mu\mathrm{NP}}$ values $-0.56 - 1.1i$ and $-0.67 + 1.1i$, respectively. It can be seen from the left plot that the values of $A_{CP}(q^2)$ can be as large as ∼20% very close to the resonance peaks and an enhancement of ∼6–12% seems possible in the region $q^2 = [6\text{–}8]$ GeV$^2$. The $A_{CP}$ predictions flip sign due to the change in sign of $\mathrm{Im}[C_9^{\mu\mathrm{NP}}]$ in NP1 and NP2, and also would change sign if one chooses Branch B for the phases.

In the right panel, we present $A_{CP}$ predictions in Scenario III for all phase choices given in Eq. (20) considering a benchmark point, $C_9^{\mu\mathrm{NP}} = -C_{10}^{\mu\mathrm{NP}} = -0.4 - 0.8i$ corresponding to maximal allowed $\mathrm{Im}[C_9^{\mu\mathrm{NP}}]$ value. This scenario allows only negative values of $\mathrm{Im}[C_9^{\mu\mathrm{NP}}]$ in the $1\sigma$ region, hence enhancement in $A_{CP}$ in the $q^2 =$ 16–17 GeV$^2$ bin is only in the positive direction for all four phase values as seen in the plot. However, Scenario I allows both positive and negative values of $A_{CP}$ in this bin. Hence, a future measurement of $A_{CP}$ in this bin can lead to potentially distinguishing signature of Scenarios I and III, irrespective of the ambiguity in the strong phase.

LHCb has measured $A_{CP}$ in 17 bins in the $q^2 =$ [0.1–22] GeV$^2$ region, while vetoing the regions [8, 11] and [12.5, 15.0] around the $c\bar{c}$ resonances. While there is a larger enhancement in the $A_{CP}(q^2)$ predictions near the $c\bar{c}$ resonances as shown in Fig. 3, this also extends further away from the resonance peaks up to $q^2 = 6$ GeV$^2$. We obtain NP predictions in the region $q^2 = [8, 9]$ GeV$^2$ near the $c\bar{c}$ resonance, and also in $q^2 = [6, 7]$ GeV$^2$ bins where LHCb measurement already exists, albeit with larger uncertainties. The binned *CP* asymmetry is defined as

$$A_{CP}[q^2_{\mathrm{min}}, q^2_{\mathrm{max}}] = \frac{\bar{\Gamma}(B^- \to K^- \mu\mu) - \Gamma(B^+ \to K^+ \mu\mu)}{\bar{\Gamma}(B^- \to K^- \mu\mu) + \Gamma(B^+ \to K^+ \mu\mu)}, \tag{21}$$

where $\Gamma = \int_{q^2_{\mathrm{min}}}^{q^2_{\mathrm{max}}} d\Gamma/dq^2$ is the binned decay rate. For the binned $A_{CP}$ predictions, we consider one of the branches, as the other branch only flips the signs of $A_{CP}$ in the presence of new complex phases. This is because the phase of $J/\psi$ changes sign in Branch B, and $A_{CP}$ prediction depends on the NP complex phase and the strong phase in the resonance region as $A_{CP} \propto \mathrm{Im}[C_9^{\mathrm{NP}}] \sin\delta_V$ [28]. We consider Branch A and Solution 1a in our analyses.

In Fig. 4, we show the predictions of integrated $A_{CP}$ superposed on the $1\sigma$ allowed region in the plane of $Z'$ couplings $\mathrm{Im}[g_{bs}]$ and $g_L^{\mu}$ for NP Scenarios I and III. We obtain the NP predictions of $A_{CP}$ in the $q^2 = [6, 7]$ GeV$^2$ and $q^2 = [8, 9]$ GeV$^2$ bins by varying the values of couplings $\mathrm{Re}[g_L^{bs}], \mathrm{Im}[g_L^{bs}]$ and $g_L^{\mu}$ in their $1\sigma$ allowed regions for Scenarios I and III. We find that the $1\sigma$ favored region in Scenario I allows for an enhancement in $A_{CP}$ both

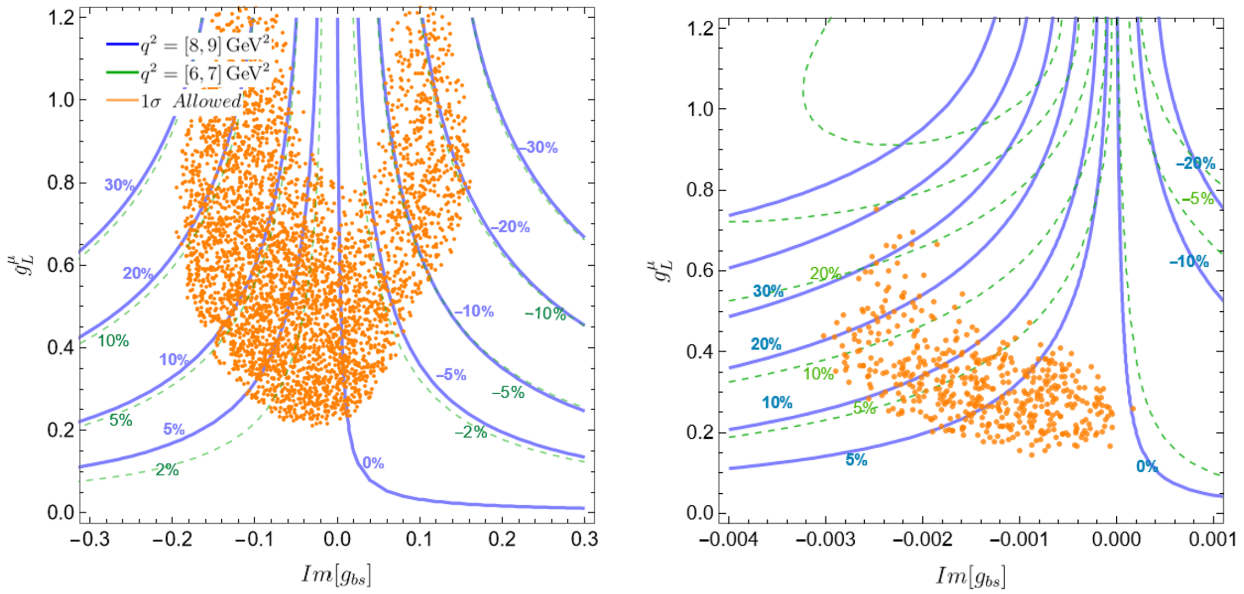


FIG. 4. The $1\sigma$ favored region (orange) in parameter space of $Z'$ couplings $\mathrm{Im}[g_{bs}]$ and $g_L^\mu$ for Scenarios I (left) and III (right). The green dashed and blue contours denote the integrated $A_{CP}$ values in the $q^2 = [6,7]$ GeV$^2$ and $q^2 = [8,9]$ GeV$^2$ bins, respectively.

in positive and negative directions up to ∼25% in the $q^2 = [8,9]$ GeV$^2$ bin when we consider Solution 1a (Branch A) for the strong phases. However, Scenario III allows only positive values of $A_{CP}$ for this choice of phase. These $A_{CP}$ predictions will flip signs for the phases in Branch B so that Scenario III will allow only negative values of $A_{CP}$. Thus, although the predictions of $A_{CP}$ in this bins have different signs for Scenarios I and III, the measurements would not be conclusive in distinguishing the two scenarios due to an ambiguity in the $J/\psi$ phase determination.

Considering branch A, similar enhancement in $A_{CP}$ of up to $\pm 15\%$ is allowed in the $q^2 = [6,7]$ GeV$^2$ bin for Scenario I, and $+20\%$ in Scenario III. For the $q^2 = [10,11]$ GeV$^2$ bin, we find an enhancement of the same order as in $q^2 = [8,9]$ GeV$^2$ bin but with the $A_{CP}$ signs flipped for the phase choices in branch A.

The negative and positive values of $A_{CP}$ arise from the positive and negative NP phases, respectively. This is true for both the $J/\psi$ and $\psi(2S)$ phase choices in Solution 1a and Solution 2a [Eq. (20)], since the sign flip of $A_{CP}$ in Solution 2a happens only above $q^2 = 10$ GeV$^2$.

Our choice of branch A is also motivated from the theory prediction of Ref. [49]. In this the nonlocal hadronic matrix element for $B \to K\ell\ell$ is split into contributions from different flavors of the quark interacting with the virtual photon, and expressed in terms of hadronic dispersion relations. In this work, the phases of $J/\psi, \psi(2S)$ are varied and a fit to the complex parameters in the dispersion relations is performed. This fit shows that a best-fit for these complex parameters is obtained for a negative value of the $J/\psi$ phase.

Considering the allowed ranges of $Z'$ couplings up to $2\sigma$, we find that the maximum range of $A_{CP}$ in Scenario III is up to $-5\%$ in the $q^2 = [8,9]$ GeV$^2$ bin. Hence, any nonzero negative $A_{CP}$ values more than a few percent in the $q^2 = [8,9]$ GeV$^2$ and $q^2 = [6,7]$ GeV$^2$ bins would indicate a strong preference to $Z'$ models generating Scenario I alone. This conclusion depends on the choice of the strong phase and holds only if the $J/\psi$ phase is negative (Branch A). Since the values of strong phases are known only up to a sign, any conclusion about distinguishing signatures of the two models is difficult in these bins as $A_{CP}$ flips sign due to the change in the phase. One promising measurement is $A_{CP}$ in the $q^2 = 16$–$17$ GeV$^2$ where Scenario III only allows positive values irrespective of the choice of phase while Scenario I allows both positive and negative values.

The positive values of $A_{CP}$ point towards $\mathrm{Im}[C_9^{\mathrm{NP}}] < 0$, which is also preferred by the current measurements of $CP$-asymmetric angular observables $A_7$, $A_8$ and $A_9$. These observables can also provide promising signatures of new physics. The differential distribution of $B \to K^{*0}\mu^+\mu^-$ decay in terms of kinematic variable $q^2$ and three angular variables, can be expressed in terms of angular coefficients $I_j$ which depend on $q^2$ and form factors. Using these, one can define $CP$-conserving and $CP$-violating observables as follows:

$$S_i(q^2) = \frac{I_i(q^2) + \bar{I}_i(q^2)}{d(\Gamma + \bar{\Gamma})/dq^2}, \quad A_i(q^2) = \frac{I_i(q^2) - \bar{I}_i(q^2)}{d(\Gamma + \bar{\Gamma})/dq^2}, \tag{22}$$

where the coefficients $\bar{I}_i$ correspond to conjugate process involving $B_0$ meson. The $CP$-asymmetric observables $A_{3,4,5}$, $A_6$, and $A_{7,8,9}$ have been measured by LHCb. In Table II we present the maximum deviations in the predictions of $A_{7,8,9}$ observables allowed by the $1\sigma$ favored

TABLE II. Maximum possible deviations in the *CP*-violating observables $A_{7,8,9}$ allowed by the $1\sigma$ favored regions of the $Z'$ models generating Scenarios I and III.

| | Low $q^2$ | | | High $q^2$ | | |
|---|---|---|---|---|---|---|
| $Z'$ Model | $A_7$ | $A_8$ | $A_9$ | $A_7$ | $A_8$ | $A_9$ |
| Sc-I | [0, 0.3]% | [−6, 5]% | [−0.6, 0.5]% | 0% | [−0.3, 0.3]% | [−0.3, 0.3]% |
| Sc-III | [−1, −12]% | [0, −6]% | [0, −0.8]% | [0, −0.6]% | [0, −0.4]% | [0, −0.3]% |

regions in the $Z'$ models generating Scenarios I and III. We find that in the low $q^2$ region, the $Z'$ model corresponding to Scenario I can give rise to a large ($\pm 5\%$) deviation in $A_8$, while Scenario III causes deviation only in the negative direction up to $-6\%$. Only Scenario III allows for a large deviation in $A_7$ in the range of $[-1, -12\%]$, making it a distinguishing feature from Scenario I. Further, in the high $q^2$ region, a deviation of up to $-0.6\%$ in $A_7$ is possible in Scenario III, while no such deviation is allowed in Scenario I. The deviations in $A_8$ and $A_9$ observables are less than 0.5% for both these scenarios, making these difficult to observe in the future. Hence, we find that future precise measurements of $A_7$ and $A_8$ observables in the low-$q^2$ bins can provide potentially interesting signatures to distinguish between the two favored $Z'$ models.

## VI. CONCLUSIONS

The $b \to s\ell\ell$ data prior to the December 2022 update showed a deviation in the LFU ratios $R_K$ and $R_{K^*}$ from their SM predictions by about $3\sigma$. This picture changed when the updated measurements of these ratios were found to be consistent with the SM predictions within $1\sigma$, thereby indicating possible electron-muon universality in the new physics scenarios. We perform a model-independent global fit considering the then favored NP scenarios in order to determine if they continue to provide a good fit to the data after the LHCb update. Assuming *CP*-violating NP, we find an overall reduction in the pull of the scenarios $C_9^{\mu\mathrm{NP}} < 0$ and $C_9^{\mu\mathrm{NP}} = -C_{10}^{\mu\mathrm{NP}}$ compared to previous fits, however the latter scenario is now less favored due to the updated measurement of $\mathrm{Br}(B_s \to \mu\mu)$ being close to the SM prediction. Introducing NP in the electron sector, we find that the scenario $C_9^{\mu\mathrm{NP}} = C_9^{e\mathrm{NP}}$ with LFU NP provide a good solution, however NP with different electron and muon couplings like in Scenario III is also allowed by the current data. We find that the current $b \to s\ell\ell$ data allows for NP WCs to be complex, with violation of electron and muon universality, and the imaginary parts to be atleast as large as the real ones. Hence, the $Z'$ and leptoquark models generating these favored NP scenarios can have complex couplings, providing new sources of *CP* violation and the signatures of these models can be studied through future measurements of *CP*-asymmetric observables.

We determine the $1\sigma$ allowed region for the two classes of $Z'$ models generating the favored NP scenarios $\mathrm{Re}[C_9^{\mu\mathrm{NP}}] < 0$ and $[C_9^{\mu\mathrm{NP}} = -C_{10}^{\mu\mathrm{NP}}, C_9^{e\mathrm{NP}} = -C_{10}^{e\mathrm{NP}}]$ using constraints from the updated measurements of all $b \to s\ell\ell$ observables, $B_s - \bar{B}_s$ mixing, mixing-induced *CP* asymmetry, and *CP*-asymmetric angular observables. We explore the possibility of using the predictions of direct *CP* asymmetry near the $c\bar{c}$ resonance to distinguish between these two classes of $Z'$ models. We find that an enhancement in $A_{CP}$ up to $\pm 25\%$ and $\pm 15\%$ in the $q^2 = [8, 9]\ \mathrm{GeV}^2$ and $q^2 = [6, 7]\ \mathrm{GeV}^2$ bins respectively is allowed by the favored parameter space of $Z'$ model generating the scenario $\mathrm{Re}[C_9^{\mu\mathrm{NP}}] < 0$, for negative value of $J/\psi$ phase. The $1\sigma$ favored parameter space of these models for the $[C_9^{\mu\mathrm{NP}} = -C_{10}^{\mu\mathrm{NP}}, C_9^{e\mathrm{NP}} = -C_{10}^{e\mathrm{NP}}]$ scenario allows for only positive values of $A_{CP}$ in these bins, for this choice of $J/\psi$ phase. However, the sign of $A_{CP}$ flips depending on the choices of the sign of $J/\psi$ phase, hence a reliable estimate of these phases is crucial in order for a future measurements in these $q^2$ bins to observe distinct features of the two $Z'$ models. Above the $J/\psi$ phase, $A_{CP}$ predictions in $q^2 = [16, 17]\ \mathrm{GeV}^2$ bin for Scenario III allows enhancement only in the positive direction for all the four phase choices while Scenario I allows both positive and negative values. Hence, $A_{CP}$ measurement in this bin is potentially interesting to probe distinctive features of the models independent of the choice of $J/\psi$ phase. When the allowed range of couplings in $Z'$ model generating Scenario III is extended to $2\sigma$, a deviation in $A_{CP}$ up to $+5\%$ is possible while any larger deviation in the positive direction is only allowed in Scenario I.

We also find potentially distinguishing features in the predictions of *CP*-asymmetric angular observables $A_7$ and $A_8$ in the low-$q^2$ region, irrespective of the strong phase determinations. Hence future high-precision measurements of *CP* asymmetric observables in $b \to s\mu\mu$ decays, would enable to obtain useful constraints on new *CP*-violating phases and help in distinguishing different favored $Z'$ models.

## ACKNOWLEDGMENTS

I would like to thank Namit Mahajan, Amol Dighe and Ashutosh Kumar Alok for useful discussions and comments on the manuscript. I also acknowledge support from the Department of Science and Technology (DST), India, under Grant No. IFA22-PH 296 (INSPIRE Faculty Award).

[1] R. Aaij *et al.* (LHCb Collaboration), Test of lepton universality in beauty-quark decays, Nat. Phys. **18**, 277 (2022).

[2] R. Aaij *et al.* (LHCb Collaboration), Test of lepton universality with $B^0 \to K^{*0}\ell^+\ell^-$ decays, J. High Energy Phys. 08 (2017) 055.

[3] R. Aaij *et al.* (LHCb Collaboration), Test of lepton universality in $b \to s\ell^+\ell^-$ decays, Phys. Rev. Lett. **131**, 051803 (2023).

[4] R. Aaij *et al.* (LHCb Collaboration), Measurement of lepton universality parameters in $B^+ \to K^+\ell^+\ell^-$ and $B^0 \to K^{*0}\ell^+\ell^-$ decays, Phys. Rev. D **108**, 032002 (2023).

[5] R. Aaij *et al.* (LHCb Collaboration), Tests of lepton universality using $B^0 \to K^0_S\ell^+\ell^-$ and $B^+ \to K^{*+}\ell^+\ell^-$ decays, Phys. Rev. Lett. **128**, 191802 (2022).

[6] R. Aaij *et al.* (LHCb Collaboration), Angular analysis and differential branching fraction of the decay $B^0_s \to \phi\mu^+\mu^-$, J. High Energy Phys. 09 (2015) 179.

[7] R. Aaij *et al.* (LHCb Collaboration), Branching fraction measurements of the rare $B^0_s \to \phi\mu^+\mu^-$ and $B^0_s \to f'_2(1525)\mu^+\mu^-$- decays, Phys. Rev. Lett. **127**, 151801 (2021).

[8] R. Aaij *et al.* (LHCb Collaboration), Measurement of form-factor-independent observables in the decay $B^0 \to K^{*0}\mu^+\mu^-$, Phys. Rev. Lett. **111**, 191801 (2013).

[9] R. Aaij *et al.* (LHCb Collaboration), Angular analysis of the $B^0 \to K^{*0}\mu^+\mu^-$ decay using 3 fb$^{-1}$ of integrated luminosity, J. High Energy Phys. 02 (2016) 104.

[10] R. Aaij *et al.* (LHCb Collaboration), Measurement of *CP*-averaged observables in the $B^0 \to K^{*0}\mu^+\mu^-$ decay, Phys. Rev. Lett. **125**, 011802 (2020).

[11] S. Descotes-Genon, T. Hurth, J. Matias, and J. Virto, Optimizing the basis of $B \to K^*ll$ observables in the full kinematic range, J. High Energy Phys. 05 (2013) 137.

[12] S. Descotes-Genon, J. Matias, and J. Virto, Understanding the $B \to K^*\mu^+\mu^-$ anomaly, Phys. Rev. D **88**, 074002 (2013).

[13] W. Altmannshofer and D. M. Straub, New physics in $B \to K^*\mu\mu$?, Eur. Phys. J. C **73**, 2646 (2013).

[14] A. K. Alok, B. Bhattacharya, D. Kumar, J. Kumar, D. London, and S. U. Sankar, New physics in $b \to s\mu^+\mu^-$: Distinguishing models through *CP*-violating effects, Phys. Rev. D **96**, 015034 (2017).

[15] A. K. Alok, A. Dighe, S. Gangal, and D. Kumar, Continuing search for new physics in $b \to s\mu\mu$ decays: Two operators at a time, J. High Energy Phys. 06 (2019) 089.

[16] W. Altmannshofer and P. Stangl, New physics in rare B decays after Moriond 2021, Eur. Phys. J. C **81**, 952 (2021).

[17] A. Carvunis, F. Dettori, S. Gangal, D. Guadagnoli, and C. Normand, On the effective lifetime of $B_s \to \mu\mu\gamma$, J. High Energy Phys. 12 (2021) 078.

[18] M. Algueró, B. Capdevila, S. Descotes-Genon, J. Matias, and M. Novoa-Brunet, $b \to s\ell^+\ell^-$ global fits after $R_{K_S}$ and $R_{K^{*+}}$, Eur. Phys. J. C **82**, 326 (2022).

[19] L.-S. Geng, B. Grinstein, S. Jäger, S.-Y. Li, J. Martin Camalich, and R.-X. Shi, Implications of new evidence for lepton-universality violation in $b \to s\ell^+\ell^-$ decays, Phys. Rev. D **104**, 035029 (2021).

[20] T. Hurth, F. Mahmoudi, D. M. Santos, and S. Neshatpour, More indications for lepton nonuniversality in $b \to s\ell^+\ell^-$, Phys. Lett. B **824**, 136838 (2022).

[21] A. Angelescu, D. Bečirević, D. A. Faroughy, F. Jaffredo, and O. Sumensari, Single leptoquark solutions to the B-physics anomalies, Phys. Rev. D **104**, 055017 (2021).

[22] R. Fleischer, E. Malami, A. Rehult, and K. K. Vos, New perspectives for testing electron-muon universality, J. High Energy Phys. 06 (2023) 033.

[23] N. R. Singh Chundawat, *CP* violation in $b \to s\ell\ell$: A model independent analysis, Phys. Rev. D **107**, 075014 (2023).

[24] R. Aaij *et al.* (LHCb Collaboration), Measurement of *CP* asymmetries in the decays $B^0 \to K^{*0}\mu^+\mu^-$ and $B^+ \to K^+\mu^+\mu^-$, J. High Energy Phys. 09 (2014) 177.

[25] L. Di Luzio, M. Kirk, A. Lenz, and T. Rauh, $\Delta M_s$ theory precision confronts flavour anomalies, J. High Energy Phys. 12 (2019) 009.

[26] N. Kovsnik and A. Smolkovivc, Lepton flavor universality and *CP* violation in an $S_3$ leptoquark model, Phys. Rev. D **104**, 115004 (2021).

[27] A. K. Alok, A. Dighe, S. Gangal, and D. Kumar, Predictions for $B_s \to \bar{K}^*\ell\ell$ in non-universal $Z'$ models, Eur. Phys. J. C **80**, 682 (2020).

[28] D. Bečirević, S. Fajfer, N. Košnik, and A. Smolkovič, Enhanced *CP* asymmetries in $B \to K\mu^+\mu^-$, Eur. Phys. J. C **80**, 940 (2020).

[29] M. Aaboud *et al.* (ATLAS Collaboration), Angular analysis of $B^0_d \to K^*\mu^+\mu^-$ decays in $pp$ collisions at $\sqrt{s} = 8$ TeV with the ATLAS detector, J. High Energy Phys. 10 (2018) 047.

[30] A. M. Sirunyan *et al.* (CMS Collaboration), Measurement of angular parameters from the decay $B^0 \to K^{*0}\mu^+\mu^-$ in proton-proton collisions at $\sqrt{s} = 8$ TeV, Phys. Lett. B **781**, 517 (2018).

[31] J. P. Lees *et al.* (*BABAR* Collaboration), Measurement of the $B \to X_s l^+ l^-$ branching fraction and search for direct *CP* violation from a sum of exclusive final states, Phys. Rev. Lett. **112**, 211802 (2014).

[32] Y. S. Amhis *et al.* (Heavy Flavor Averaging Group and HFLAV Collaboration), Averages of b-hadron, c-hadron, and $\tau$-lepton properties as of 2021, Phys. Rev. D **107**, 052008 (2023).

[33] V. Khachatryan *et al.* (CMS Collaboration), Angular analysis of the decay $B^0 \to K^{*0}\mu^+\mu^-$ from pp collisions at $\sqrt{s} = 8$ TeV, Phys. Lett. B **753**, 424 (2016).

[34] R. Aaij *et al.* (LHCb Collaboration), Differential branching fractions and isospin asymmetries of $B \to K^{(*)}\mu^+\mu^-$ decays, J. High Energy Phys. 06 (2014) 133.

[35] R. Aaij *et al.* (LHCb Collaboration), Angular analysis of the $B^0 \to K^{*0}e^+e^-$ decay in the low $q^2$ region, J. High Energy Phys. 04 (2015) 064.

[36] S. Wehle *et al.* (Belle Collaboration), Lepton-flavor-dependent angular analysis of $B \to K^*\ell^+\ell^-$, Phys. Rev. Lett. **118**, 111801 (2017).

[37] D. M. Straub, flavio: A Python package for flavour and precision phenomenology in the standard model and beyond arXiv:1810.08132.

[38] W. Altmannshofer, S. Gori, M. Pospelov, and I. Yavin, Quark flavor transitions in $L_\mu - L_\tau$ models, Phys. Rev. D **89**, 095033 (2014).

[39] D. Aristizabal Sierra, F. Staub, and A. Vicente, Shedding light on the $b \to s$ anomalies with a dark sector, Phys. Rev. D **92**, 015001 (2015).

[40] S. R. Mishra *et al.* (CCFR Collaboration), Neutrino tridents and W Z interference, Phys. Rev. Lett. **66**, 3117 (1991).
[41] W. Altmannshofer, S. Gori, J. Martín-Albo, A. Sousa, and M. Wallbank, Neutrino tridents at DUNE, Phys. Rev. D **100**, 115029 (2019).
[42] S. Schael *et al.* (ALEPH, DELPHI, L3, OPAL, and LEP Electroweak Collaborations), Electroweak measurements in electron-positron collisions at W-boson-pair energies at LEP, Phys. Rep. **532**, 119 (2013).
[43] J. A. Bailey *et al.*, $B \to K l^+ l^-$ decay form factors from three-flavor lattice QCD, Phys. Rev. D **93**, 025026 (2016).
[44] F. Kruger and L. M. Sehgal, Lepton polarization in the decays $B \to X_s \mu^+ \mu^-$ and $B \to X_s \tau^+ \tau^-$, Phys. Lett. B **380**, 199 (1996).
[45] P. A. Zyla *et al.* (Particle Data Group), Review of particle physics, Prog. Theor. Exp. Phys. **2020**, 083C01 (2020).
[46] M. Beneke, C. Bobeth, and Y.-M. Wang, $B_{d,s} \to \gamma \ell \overline{\ell}$ decay with an energetic photon, J. High Energy Phys. 12 (2020) 148.
[47] M. Beneke, T. Feldmann, and D. Seidel, Systematic approach to exclusive $B \to V l^+ l^-$, $V\gamma$ decays, Nucl. Phys. **B612**, 25 (2001).
[48] R. Aaij *et al.* (LHCb Collaboration), Measurement of the phase difference between short- and long-distance amplitudes in the $B^+ \to K^+ \mu^+ \mu^-$ decay, Eur. Phys. J. C **77**, 161 (2017).
[49] A. Khodjamirian, T. Mannel, and Y. M. Wang, $B \to K \ell^+ \ell^-$ decay at large hadronic recoil, J. High Energy Phys. 02 (2013) 010.